nature communications

Article

https://doi.org/10.1038/s41467-024-55261-3

ALCAM is an entry factor for severe community acquired Pneumonia-associated Human adenovirus species B

Received: 26 March 2024

Accepted: 5 December 2024

Published online: 30 December 2024

Check for updates

Yusang Xie[1,6], Hong Mei[2,6], Wei Wang[2], Xiao Li[3], Pengfei Hu[2], Xingui Tian[3], Rong Zhou[3,4], Jia Liu[2,4,5] ✉ & Jieming Qu[1] ✉

Human adenovirus (HAdV) is a widely spread respiratory pathogen that can cause infections in multiple tissues and organs. Previous studies have established an association between HAdV species B (HAdV-B) infection and severe community-acquired pneumonia (SCAP). However, the connection between SCAP-associated HAdV-B infection and host factor expression profile in patients has not been systematically investigated. Here, we perform a CRISPR genetic screen on HAdV-B using two generations of cell surface protein-focused CRISPR libraries and identify a series of host factors including the known receptor DSG-2 and an unknown factor, activated leukocyte cell adhesion molecule (ALCAM). Further investigation shows that ALCAM affects HAdV-B infection by participating in viral internalization. Transcriptomics data from human blood samples suggests that ALCAM expression is higher in SCAP patients with HAdV-B infection than in those with other infections. Chimeric and authentic virus experiments show that ALCAM is a widely used host factor across B1 and B2 genetic clusters of HAdV-B. The dissociation constant between the knob domain of HAdV-B fiber and ALCAM is 837 nM in average. In summary, our results suggest that ALCAM is an entry factor for SCAP-associated HAdV-B.

Adenoviruses (AdVs) are non-enveloped, icosahedral viruses with a linear, double-stranded DNA genome ranging from 26 to 45 kb[1,2]. The viral particle is 70 to 100 nm in size and the capsid is composed of 240 hexons and 12 pentons. Five penton base proteins form a capsomere that supports a trimeric fiber protein. The fiber protein includes three structural domains: tail, shaft, and knob[2].

AdV belongs to the *Adenoviridae* family that can infect various vertebrates including mammals, birds, fish, reptiles and amphibians. Human adenoviruses (HAdVs) are classified into the genus *Mastadenovirus* which are spread among mammal hosts[1,2]. HAdVs can cause a wide range of infections in respiratory, ocular, gastrointestinal and other tissues. There are over 100 known serotypes of HAdVs, categorized into seven species A to G based on their genetic and antigenic properties[1]. Certain serotypes of HAdVs are associated with pulmonary infections, typically present with mild upper respiratory symptoms. However, HAdV species B (HAdV-B) have been reported to cause severe pneumonia and life-threatening complications necessitating intensive care unit admission in all ages[3] including children[4,5] and

[1]Department of Pulmonary and Critical Care Medicine, Ruijin Hospital, Institutes of Respiratory Diseases, School of Medicine, Shanghai Jiao Tong University and Shanghai Key Laboratory of Emergency Prevention, Diagnosis and Treatment of Respiratory Infectious Diseases, Shanghai, China. [2]Shanghai Institute for Advanced Immunochemical Studies and School of Life Science and Technology, ShanghaiTech University, Shanghai, China. [3]State Key Laboratory of Respiratory Disease, National Clinical Research Center for Respiratory Disease, Guangzhou Institute of Respiratory Health, The First Affiliated Hospital of Guangzhou Medical University, Guangzhou Medical University, Guangzhou, China. [4]Guangzhou National Laboratory, Guangzhou International Bio Island, No. 9 XingDaoHuanBei Road, Guangzhou, Guangdong, China. [5]Shanghai Clinical Research and Trial Center, Shanghai, China. [6]These authors contributed equally: Yusang Xie, Hong Mei. ✉e-mail: liujia@shanghaitech.edu.cn; jmqu0906@163.com

young adults[6], both with and without compromised immune conditions[2,7]. HAdV-B are further divided into two genetic clusters, including B1 (HAdV3, HAdV7, HAdV16, HAdV21 and HAdV50) and B2 (HAdV11p, HAdV14, HAdV34 and HAdV35)[1,2]. In our recent multi-center prospective etiology study in 2022 in China, HAdVs appeared to be the second most prevalent viral pathogen causing severe community-acquired pneumonia (SCAP), among which HAdV-B7 was the dominant serotype (8 out of 12, 66.7%)[8].

HAdV-A, C, D, E and F, but not species B, use an immunoglobulin superfamily protein coxsackievirus and adenovirus receptor (CAR) as the primary receptor for infection[9,10]. It has been reported that HAdV-B11, HAdV-B16, HAdV-B21, HAdV-B35 and HAdV-B50 use CD46 as a receptor[11], while HAdV-B3, HAdV-B7, HAdV-B11 and HAdV-B14 utilize desmoglein-2 (DSG-2) as a high-affinity receptor[12,13]. DSG-2 is a cell adhesion molecule belonging to the cadherin superfamily[14], with a similar adhesion function to CAR. In addition, several other cellular molecules have been reported to interact with HAdV-B to facilitate its infection, including heparin sulfate proteoglycans[15], integrins[16], CD80 and CD86[17]. However, the receptor usage profile of HAdV-B remains to be explored because loss of function analysis of previously identified receptor did not seem to abolish viral infection[12], indicating that other cellular proteins may be involved in the infection process.

In order to investigate the host factors of HAdV-B in a systematic approach, we sought to perform CRISPR-based forward genetic screen on HAdV-B. Genome-wide CRISPR screens have been widely used to identify novel host factors of emerging and important pathogens, including SARS-CoV-2[18,19], Rift Valley fever virus[20], Chikungunya virus[21] and others. In addition, CRISPR libraries focusing on a subset of gene list has been applied for the discovery of virus host factors[22]. In a previous study, we constructed a focused CRISPR library containing approximately 1400 cell surface proteins, referred to as surfaceome CRISPR (SfCRISPR) library hereafter, and showed that this library could efficiently identify host factors of rhinovirus[23].

In the present study, we constructed a second-generation SfCRISPR library containing around 5600 cell surface proteins and performed a genetic screen on HAdV-B infection using both first and second generations of SfCRISPR libraries (SfCRISPR-v1 and -v2). We identified activated leukocyte cell adhesion molecule (ALCAM), a member of the immunoglobulin superfamily that is present in various cell types[24], as a functional receptor involving in HAdV-B internalization. Subsequent analyses uncovered the clinical relevance between ALCAM expression and SCAP-associated HAdV-B infection and illustrated the pattern of interactions between ALCAM and HAdV-B fiber protein.

Results

Identification of HAdV species B in SCAP patients

In a previous prospective multi-center observational study of SCAP involving 17 hospitals and 10 regions of mainland China (Supplementary Fig. 1a), human adenovirus (HAdV) was identified as the second most frequently seen virus in severe patients with identifiable pathogen infections (12 out of 198) (Fig. 1a)[8]. In the present study, we performed a more detailed analysis on the serotypes of these HAdV strains and identified the presence of HAdV-B3, B7 and B55, with B7 being the predominant strain in 8 out of 12 patients (66.7%).

Investigation of the receptor usage of HAdV-B can be important for understanding the molecular basis for its distribution in SCAP patients. It is well known that unlike species C HAdV, species B does not use CAR as the entry receptor[9,25]. Instead, HAdV-B infection relies on CD46[11] or DSG-2[12,13], and specifically HAdV-B7 uses DSG-2 as an entry receptor[12,13]. Therefore, we re-analyzed the transcriptome-wide RNA expression in the blood samples of SCAP patients as reported in the previous study (Supplementary Fig. 1a)[26] to dissect the association between DSG-2 expression and HAdV-B infection. It was found that SCAP patients with HAdV infection did not have significantly higher DSG-2 expression than those with other infections (Fig. 1b). This observation suggested that DSG-2 might not be the dominating factor for HAdV-B infection and prompted us to investigate whether other receptors could be responsible for the liability of HAdV-B infection in SCAP patients.

Construction of chimeric human adenovirus-B7 (HAdV-C5/B7) containing HAdV-B7 fiber

To investigate the receptor usage of HAdV-B, we intended to construct HAdV-C5-based chimeric virus with substituted fiber protein from HAdV-B7 (Supplementary Fig. 1b), which was deemed to be responsible for HAdV attachment and entry[27]. We compared several publicly available sequences of HAdV-B7 and found that their fiber proteins had a few amino acid variations (Supplementary Fig. 1c). We chose a HAdV-B7 strain identified in Beijing, China (GenBank: KX897164) and replaced the shaft and knob domains of HAdV-C5 with those of this B7 strain (Supplementary Fig. 2a). The chimeric HAdV-B7 virus (HAdV-C5/B7) was produced using commercially available HAdV-C production system.

HAdV-C5/B7 virus contained a GFP transgene (HAdV-C5/B7-GFP) and was found to be capable of efficiently infecting HEK-293A cells (Fig. 1c). To validate whether HAdV-C5/B7-GFP had a receptor usage profile different from HAdV-C5, we examined their infection on *CAR* knockout and *DSG-2* knockout cells (Supplementary Fig. 2b, c and Supplementary Fig. 3a). It was found the infection of HAdV-C5 was dependent on CAR but not DSG-2, while HAdV-C5/B7-GFP infection relied on DSG-2 but not CAR, both of which were consistent with the reported receptor usage[12,25]. The residual HAdV-C5 transduction in *CAR* knockout cells could be due to the residual cell surface expression of CAR in the mixed population of knockout cells (Supplementary Fig. 3a, b). Collectively, these results suggested that HAdV-C5/B7-GFP was constructed successfully.

Design and construction of SfCRISPR-Cas9 libraries

In our previous study, SfCRISPR-v1 library was used to identify host factors of rhinovirus[23,28]. Herein, we constructed SfCRISPR-v2 library and expanded the library size from 1344 to 5622 surface proteins. The information of the surface proteins in SfCRISPR-v2 was collected from Uniprot, GO, Human Protein Atlas and Cell Surface Protein Atlas (CSPA) databases (Fig. 1d). SfCRISPR-v2 contained 22,631 sgRNA with an average of four sgRNAs for each gene (Supplementary Data File 1). Similar to our previous work[28], these sgRNAs were designed to target protein coding regions (NCBI CCDS data)[29] and the on- and off-target scores were calculated using previously described methods[30,31] (Supplementary Fig. 4a). In the finalized library, the majority of sgRNAs had on-target scores of around 0.75 (Supplementary Fig. 4b) and off-target scores of equal to or less than 30 (Supplementary Fig. 4c).

To maximize the probability of identifying novel receptors of HAdV-B7, we used both SfCRISPR-v1 and -v2 for the screening experiment. HEK-293T cells were transduced with lentiviruses (LVs) carrying these two libraries respectively. Next-generation sequencing (NGS) analyses showed that libraries as pooled LV plasmids or as transduced cells displayed full coverage of sgRNAs (Supplementary Fig. 5a) with a uniform distribution as anticipated (Supplementary Fig. 5b, c). In addition, in order to have further quality control of transduced cells carrying the libraries, we compared the shift of sgRNAs targeting to essential and nonessential genes as previously described[32] and found that the sgRNAs targeting essential genes were significantly depleted, as compared to non-targeting sgRNAs or sgRNAs targeting non-essential genes (Supplementary Fig. 5d). Collectively, these results demonstrated that SfCRISPR-v1 and -v2 libraries were successfully contructed and qualified for the screening experiment.

https://doi.org/10.1038/s41467-024-55261-3

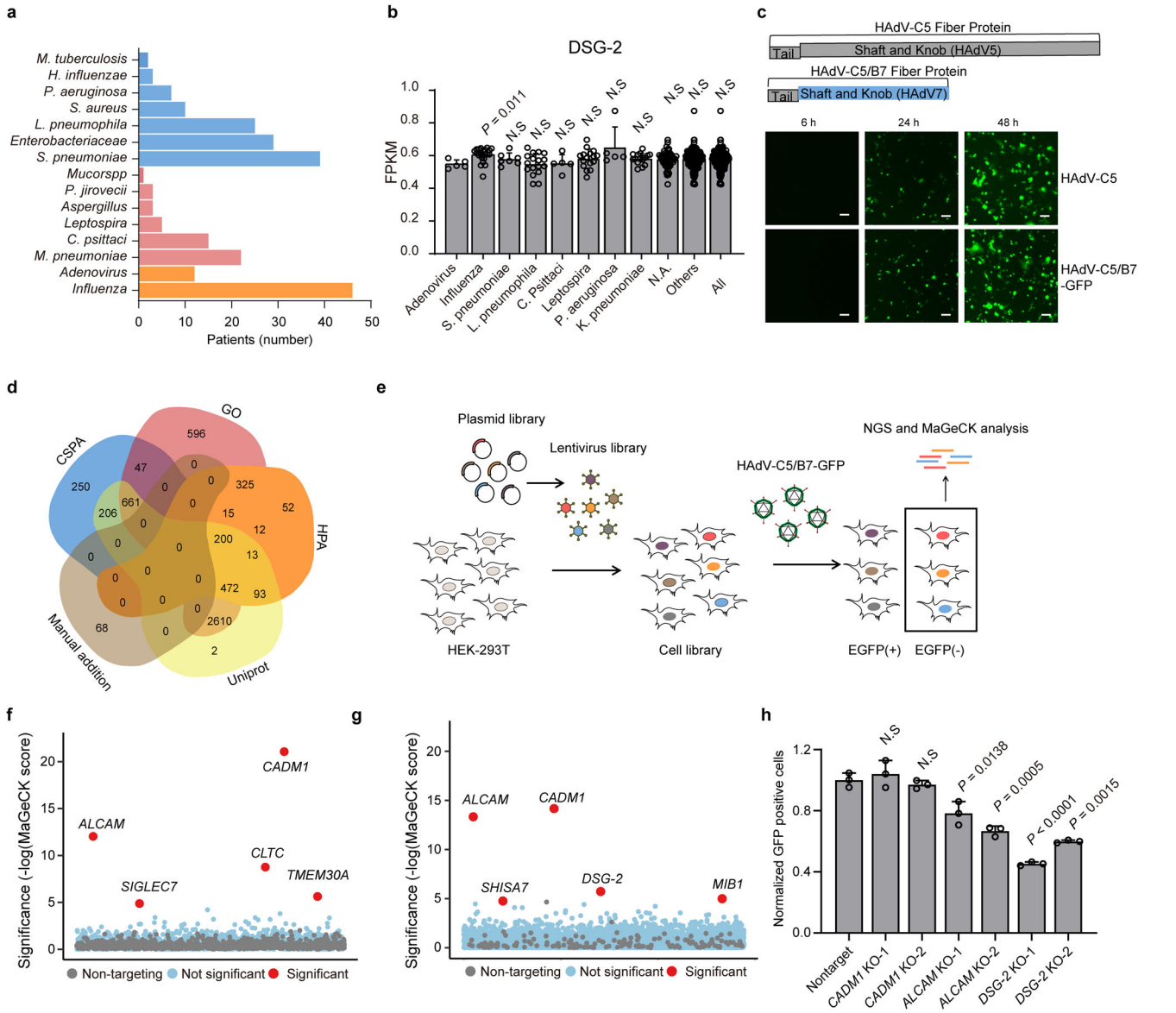

Fig. 1 | Identification of ALCAM as a host factor of HAdV-C5/B7-GFP through SfCRISPR screen in HEK-293T cells. a Analysis of SCAP-associated HAdVs. The colors are blue for bacteria, pink for atypical pathogens and orange for viruses. The data are extracted from a previous publication[8] and re-analyzed and the figure re-drawn. **b** Analysis of DSG-2 transcriptomic expression in the blood samples from SCAP patients with different pathogen infections. FPKM, fragments per kilobase of exon model per million mapped fragments. N.A., no available identifiable pathogen information. Others, all pathogens excluding HAdV. All, all analyzed SCAP patients. Data are presented as mean ± standard deviation (SD) ($n \geq 3$) from different patients. Statistical analyses are performed between HAdV group and other groups using two-tailed unpaired Student's *t* test. **c** Construction of HAdV-C5/B7-GFP and evaluation of its infection efficiency in HEK-293A, in comparison with HAdV-C5. Scale bar, 100 μm. The experiment is repeated three times independently and similar results are obtained. **d** Venn plot showing the overlap of cell surface proteins as defined by each public database. SfCRISPR-v2 contains the union set of these proteins. **e** Flow chart showing the screening procedure of GFP-negative selection in HEK-293T cells. Bubble plot showing the screening results using SfCRISPR-v1 (**f**) and -v2 (**g**) libraries. The compared groups are test and mock infections. Significance of enrichment is calculated using MAGeCK and candidate hits with FDR cut-offs of less than 0.01 are displayed. **h** Evaluation of the effects of *ALCAM*, *CADM1* and *DSG-2* knockout on HAdV-C5/B7-GFP infection in HEK-293T cells by flow cytometry. Data are presented as mean ± SD ($n = 3$) from three independent biological replicates. The significant difference between non-targeting sgRNA and knockout groups is determined using two-tailed Student's *t* test and the *P* values are shown. The *p* values between nontarget and *DSG-2* knockout-1 is 4e-5. Source data are provided as a Source Data file.

Identification of HAdV-C5/B7 host factors through surfaceome CRISPR screen

The quality controlled SfCRISPR-v1 and -v2 HEK-293T libraries were infected with HAdV-C5/B7-GFP. GFP-negative cells were sorted through flow cytometry to enrich cells that were resistant to HAdV-C5/B7-GFP infection. These enriched cells were collected, extracted for genomic DNA, PCR amplified for sgRNAs and then analyzed by NGS (Fig. 1e). The candidate genes with enriched sgRNAs were determined as described[23]. Importantly, both screens using SfCRISPR-v1 and -v2 identified HAdV-B known receptor DSG-2 among the top 10 hits (Fig. 1f, g and Supplementary Data File 2, 3). In both screens, two candidate genes, ALCAM and cell adhesion molecule 1 (CADM1), appeared as the top two hits (Fig. 1f, g). Therefore, we constructed *ALCAM* and *CADM1* knockout HEK-293T cells, along with *DSG-2* knockout cells as a control (Supplementary Fig. 3a–c). It was found that HAdV-C5/B7-GFP exhibited significantly reduced infection in *ALCAM* and *DSG-2* knockout cells, but not in *CADM1* knockout cells (Fig. 1h).

https://doi.org/10.1038/s41467-024-55261-3

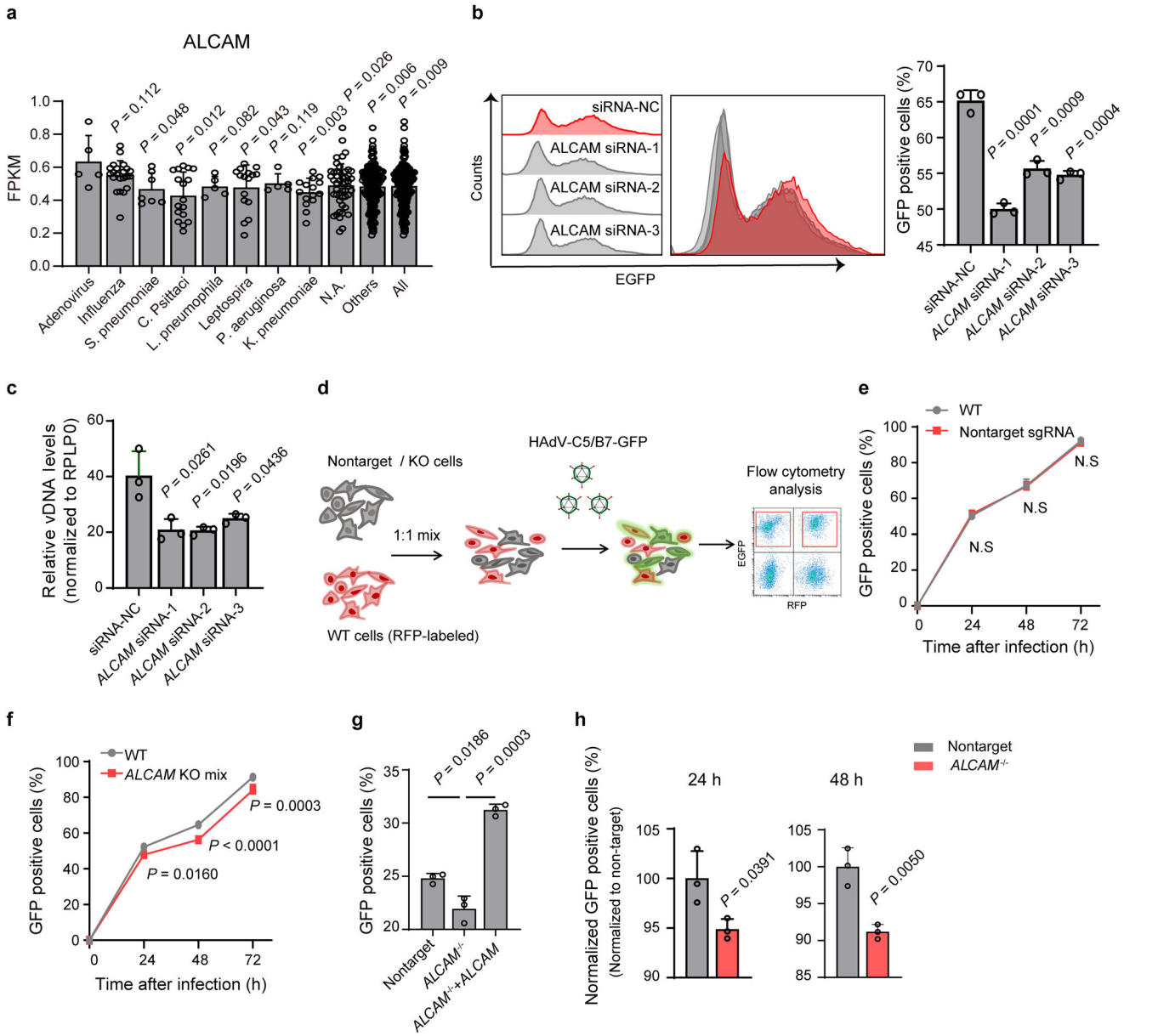

Fig. 2 | Investigation of the function of ALCAM on HAdV-C5/B7-GFP infection in HEK-293A cells. a Analysis of ALCAM transcriptomic expression in the blood samples from SCAP patients with different pathogen infections. FPKM, Fragments Per Kilobase of exon model per Million mapped fragments. N.A., no available identifiable pathogen information. Others, all pathogens excluding HAdV. All analyzed SCAP patients. Data are presented as mean ± standard deviation (SD) ($n \geq 3$) from different patients. Statistical analyses are performed between adenovirus group and other groups using two-tailed unpaired Student's *t* test. Evaluation of the effects of *ALCAM* knockdown on HAdV-C5/B7-GFP infection in HEK-293A cells, as determined by GFP fluorescence using flow cytometry (**b**) or viral L3 DNA levels using qPCR quantification (**c**). Assays are performed at 48 h post infection. NC, negative control using scrambled siRNA. Rplp0 is used as an internal control for qPCR. Data are presented as mean ± SD ($n = 3$) from three independent biological replicates. The significant difference between siRNA-NC and *ALCAM*-siRNA groups is analyzed by two-tailed unpaired Student's *t* test. **d** Flow chart showing the procedure of competition assay. The cell populations to be compared are highlighted in red boxes. Flow cytometry analysis of HAdV-C5/B7-GFP infection in the mixed population of WT cells with non-targeting (**e**) or *ALCAM* knockout (**f**) cells at 24 h, 48 h and 72 h post infection. *ALCAM* KO mix, *ALCAM* knockout on mixed population without isolation of single clones. **g** Flow cytometry analysis of HAdV-C5/B7-GFP infection in non-targeting sgRNA, $ALCAM^{-/-}$ and *ALCAM* overexpression-rescued cells at 48 h post infection. **h** Flow cytometry analysis of HAdV-C5/B7-GFP infection in the mixed population of WT cells with non-targeting sgRNA or *ALCAM* knockout single clone at 24 h and 48 h post infection in the competition asssay. For all competition experiments, WT group is used as an internal control, and non-targeting sgRNA and $ALCAM^{-/-}$ groups are normalized to WT. For e-h, data are presented as mean ± SD ($n = 3$) from three independent biological replicates. For (**e**, **f**) the significant difference is determined using two-way ANOVA with Sidak's multiple comparisons test. The *p* values between WT and *ALCAM* KO mix at 48 h post infection is 0.000098. For (**a**–**c** and **g**, **h**), the significant difference is analyzed by two-tailed unpaired Student's *t* test unless noted otherwise. Source data are provided as a Source Data file.

Validation of ALCAM as a functional host dependency factor for SCAP-associated HAdV-B7 infection

To determine the clinical significance of CADM1 and ALCAM, we re-visited the RNA-Seq data from the previous study[26]. It was found that *ALCAM* expression in SCAP patients with HAdV-B infection (Supplementary Fig. 6a, b) were significantly higher than that in patients with other infections (Fig. 2a). By contrast, no significant difference was discovered for CADM1 (Supplementary Fig. 6c). Despite of the above results, further analyses are necessary to establish a causal link between *ALCAM* expression and HAdV-B

infection. Therefore, the following experiments were focused on ALCAM protein.

We first sought to analyze the function of ALCAM for HAdV-C5/B7-GFP infection in HEK-293A, which was known to support the infective replication of HAdV-C5 due to presence of the adenoviral E1A/B genes[33]. We knocked down the expression of *ALCAM* in HEK-293A cells using three small interfering RNAs (siRNAs) (Supplementary Fig. 7a) and observed that *ALCAM* knock down reduced HAdV-C5/B7-GFP infection as determined by GFP fluorescence and viral genomic DNA L3 (Fig. 2b, c and Supplementary Fig. 7b, c).

As *ALCAM* knockout cells displayed decreased cell proliferation rate (Supplementary Fig. 7d), we sought to use competition experiments to evaluate the effects of *ALCAM* knockout on HAdV infection. In these experiments, wild-type HEK-293A cells expressing red fluorescent protein (RFP) were co-cultured in 1:1 ratio with non-targeting sgRNA control cells or *ALCAM* knockout cells, and then the mixed population of cells were infected with HAdV-C5/B7-GFP (Fig. 2d). It was found that non-targeting sgRNA cells and wild-type cells had very similar HAdV-C5/B7-GFP infection rate over a time course of 72 h post infection (Fig. 2e), while *ALCAM* knockout cells exhibited reduced rate of infection (Fig. 2f). These experiment were conducted with a mixture of wild type and knockout cells under identical micro-environment and thus verified the function of ALCAM in HAdV-C5/B7-GFP infection.

Furthermore, we constructed *ALCAM* knockout single clones (*ALCAM*$^{-/-}$) of HEK-293A cells (Supplementary Fig. 7e–g) to evaluate the effects of *ALCAM* knockout on HAdV-B infection. It was observed that *ALCAM*$^{-/-}$ cells exhibited markedly decreased HAdV-C5/B7-GFP infection and that *ALCAM* overexpression rescue in *ALCAM*$^{-/-}$ cells restored HAdV-C5/B7-GFP infection (Fig. 2g and Supplementary Fig. 7e–g). We also found that *ALCAM* overexpression in *ALCAM*$^{-/-}$ cells could rescue the minor disruptive effects of *ALCAM* knockout on cell proliferation (Supplementary 7h). We next examined HAdV-C5/B7-GFP infection in *ALCAM*$^{-/-}$ cells using the competition assays and found that *ALCAM*$^{-/-}$ cells displayed decreased infection rate at 24 h and 48 h post infection (Fig. 2h). Collectively, these results suggested that ALCAM was a functional host dependency factor for SCAP-associated HAdV-B7 infection.

Investigation of the function of ALCAM as a widely used host factor for HAdV-B

In order to examine the function of ALCAM in different HAdV-B, we constructed chimeric HAdVs as described above where the fiber protein was replaced with each previously identified HAdV-B virus (Supplementary Fig. 8a). As expected, the infection of chimeric HAdV-B viruses (HAdV-C5/B) in HEK-293A did not rely on HAdV-C5 receptor CAR (Supplementary Fig. 8b). Importantly, competition experiments showed that chimeric HAdV-B3, B11, B14 and B50, with the exception of B35, had notably reduced infection in *ALCAM*$^{-/-}$ HEK-293A cells (Fig. 3a). By contrast, HAdV-C5 infection was not inhibited by *ALCAM* knockout (Fig. 3a). These results demonstrated that the changes of HAdV-C5/B infection were directly related with the effects of *ALCAM* knockout rather than indirect effects of cell proliferation. Moreover, the observed differential effects of *ALCAM* knockout on HAdV-C5/B and HAdV-C5 also excluded the possible non-specific interactions of HAdV-C5 capsid with ALCAM protein. Collectively, these results suggested that ALCAM could act as a widely used host factor for HAdV-B.

To further evaluate the function of ALCAM in HAdV-B infection, we sought to examine the infectivity of clinical isolates of HAdV-B strains, HAdV-B3 (GenBank: DQ099432.4), -B7 (GenBank: GQ478341.1), -B14 (GenBank: JQ824845.1), and -B35 (GenBank: AY128640.2)[34] on *ALCAM*$^{-/-}$ HEK-293A cells. MEGA X-based phylogenetic analyses[35,36] using sequencing-verified fiber genes (Supplementary Fig. 8c–f) revealed that the selected clinical HAdV-B strains were closely related with the previously identified strains deposited in the public database (Fig. 3b). The infection experiments showed that *ALCAM* knockout significantly reduced viral replication of clinical HAdV-B3 and HAdV-B7 under different multiplicity of infection (MOI) (Fig. 3c, d). In addition, it was found that wild-type HAdV-B14, but not B35, had reduced replication in *ALCAM*$^{-/-}$ HEK-293A cells, which was consistent with the results of chimeric viruses (Fig. 3e). Moreover, ALCAM overexpression could restore the susceptibility of *ALCAM*$^{-/-}$ cells to HAdV-B7 infection, as evaluated by viral titers (Fig. 3f) and cytopathic effects (CPEs) (Fig. 3g).

To further examine the effects of endogenous ALCAM on HAdV-B infection, we characterized ALCAM expression in several cell lines, including HEK-293A, A549, Hela and U-87MG. It was found that HeLa cells displayed notably lower *ALCAM* mRNA expression than other cells (Supplementary Fig. 9a). We performed HAdV-B7 infection in these cells and found that HeLa cells had much lower viral titer than other cells (Supplementary Fig. 9b). Moreover, it was found that *ALCAM* overexpression in HeLa cells (Supplementary Fig. 9c, d) could significantly increase the infection of HAdV-C5/B7, but not -C5 (Fig. 3h and Supplementary Fig. 9e). Consistently, the effects of *ALCAM* overexpression on promoting virus infection was observed with clinical isolate of HAdV-B7 (Fig. 3i). These data confirmed the dependency of HAdV-B infection on ALCAM expression.

In addition, we examined HAdV-B infection in Chinese hamster ovary K1 (CHO-K1) cells which displayed high expression of an ALCAM homolog protein bearing 92.11% sequence similarity to human ALCAM (Supplementary Fig. 9f, g). It was found that HAdV-B had little infection in CHO-K1 cells (Supplementary Fig. 9h). We further overexpressed hamster's *Alcam* in *ALCAM*$^{-/-}$ HEK-293A cells and examined HAdV-B7 infection on these cells (Supplementary Fig. 9i). The results showed that hamster's ALCAM did not promote authentic HAdV-B7 infection (Supplementary Fig. 9j). Collectively, these data suggested that hamster ALCAM did not support HAdV-B infection as human ALCAM did.

ALCAM enhances HAdV-B7 internalization

We then investigated whether ALCAM was involved in HAdV-B attachment and internalization. For attachment assay, wild type or *ALCAM* KO cells were incubated with virus at 4 °C and then harvested for qPCR quantification of attached virus. For internalization assay, cells were incubated with virus first at 4 °C and then at 37 °C to trigger virus internalization. Surface-bound virus was removed by extensive washing and the internalized virus was quantified by qPCR (Supplementary Fig. 10a). It was found that *ALCAM* knockout did not affect HAdV-C5/B7 attachment but significantly reduced virus internalization, while *DSG-2* knockout affected both attachment and internalization processes (Fig. 4a). Consistently, HAdV-C5/B7 and clinical HAdV-B7 had decreased virus internalization, but not attachment, in *ALCAM*$^{-/-}$ HEK-293A single clone (Fig. 4b, c). Collectively, all these results suggested that ALCAM was an important factor for HAdV-B internalization.

Determination of the interaction pattern between ALCAM and HAdV-B fiber protein

To explore how ALCAM interacted with HAdV-B fiber protein, we co-transfected HEK-293T cells with ALCAM-myc and fiber-HA overexpression plasmids, and performed co-immunoprecipitation (Co-IP) experiments. The results confirmed that fiber protein could be co-immunoprecipitated with ALCAM (Fig. 4d). An EGFP negative control was included in the Co-IP experiments (Supplementary Fig. 10b) to improve the reliability of the results. In addition, we observed that DSG-2 could also interact with fiber protein (Supplementary Fig. 10c) though ALCAM and DSG-2 seemed to interact with HAdV-B fiber of different molecular weight. The different sizes of fiber proteins (Supplementary Fig. 10c) were likely the fragments of shaft, knob or tail or the combinations due to cellular processing of the full-length fiber.

In order to dissect the interacting domains between ALCAM and fiber proteins, we constructed truncated fiber constructs including

https://doi.org/10.1038/s41467-024-55261-3

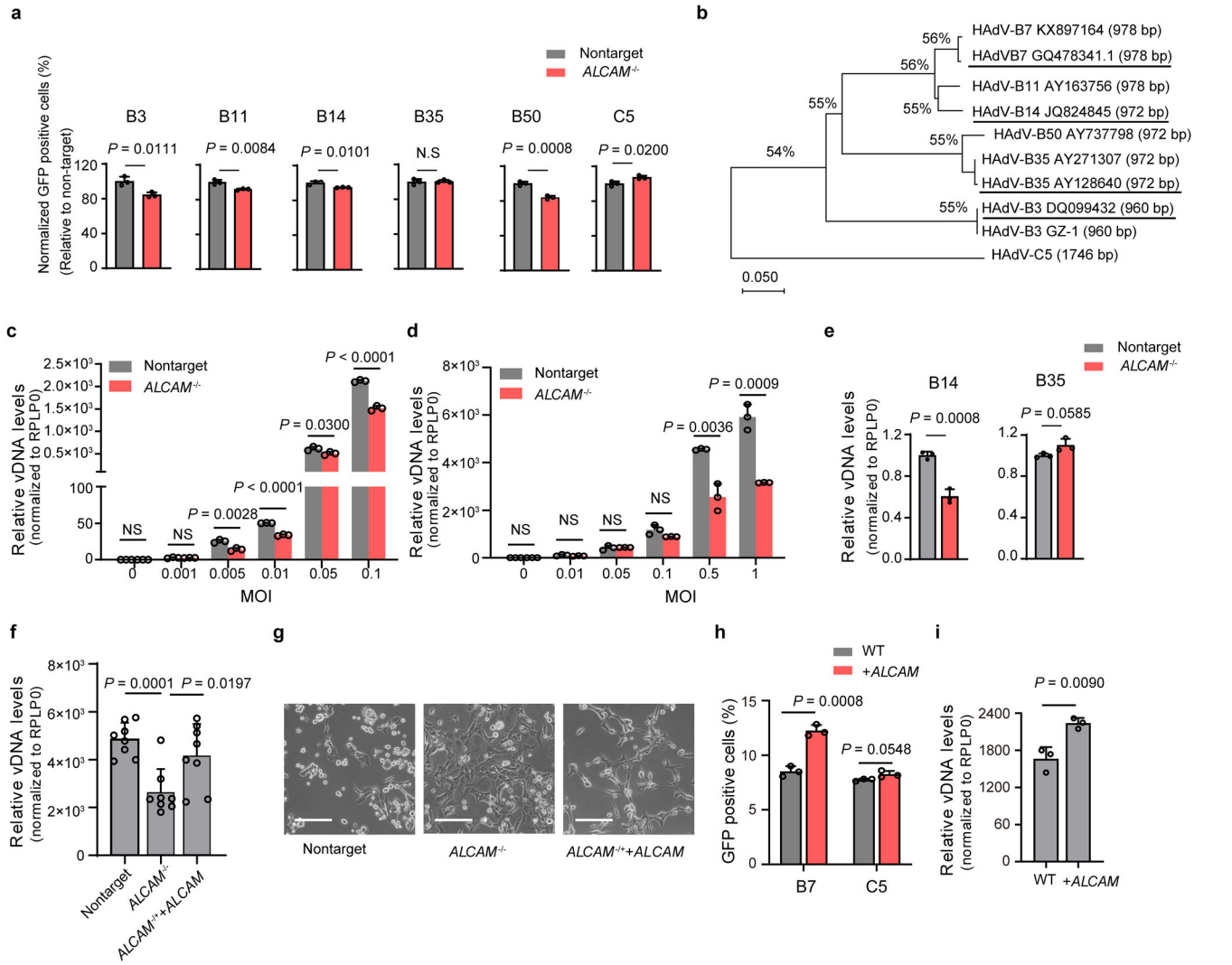

Fig. 3 | Characterization of ALCAM as a widely used host factor for HAdV-B and clinical isolates. a Flow cytometry analysis of the GFP positive ratio in the competition asssay. WT cells are mixed with non-targeting or *ALCAM*$^{-/-}$ cells and infected with HAdV-C5/B7 or HAdV-C5 for 48 h. The infection rate of each chimeric viruses in *ALCAM*$^{-/-}$ group is normalized to that in non-targeting sgRNA group. **b** Phylogenetic analyses of the clinical isolates of HAdV-B3 and -B7 using fiber gene as the reference. The clinical isolates used in this study are HAdV-B3 (GenBank: DQ099432.4), -B7 (GenBank: GQ478341.1), -B14 (GenBank: JQ824845) and -B35 (GenBank: AY128640.2), as highlighted. qPCR quantification of HAdV DNA levels in non-targeting sgRNA mock and *ALCAM*$^{-/-}$ cells at 48 h post infection with clinical HAdV-B3 (**c**) and HAdV-B7 (**d**). **e** qPCR quantification of HAdV-B14 and -B35 L5 DNA levels in non-targeting sgRNA mock and *ALCAM*$^{-/-}$ cells at 48 h post infection with HAdV-B14 and HAdV-B35 clinical isolates. **f** qPCR quantification of HAdV-B7 L5 DNA levels in non-targeting sgRNA mock, *ALCAM*$^{-/-}$ and overexpression-rescued cells at 48 h post virus infection. **g** Representive images of the CPEs in non-targeting sgRNA mock, *ALCAM*$^{-/-}$ and overexpression-rescued cells at 48 h post infection with clinical HAdV-B7. Scale bars, 100 μm. The experiment is repeated three times independently and similar results are obtained. **h** The effects of *ALCAM* overexpression on HAdV-C5/B7-GFP infection in Hela cells, as evaluated by flow cytometry quantification of GFP fluorescence. **i** qPCR quantification of viral L5 DNA levels in WT and *ALCAM*-overexprssed HeLa cells at 48 h post infection with clinical HAdV-B7. For (**c**–**f** and **i**), rplp0 is used as an internal control. For (**a**, **c**–**f** and **h**, **i**), data are presented as mean ± SD ($n \geq 3$) from independent biological replicates. For (**c**), the *p* values between non-targeting sgRNA mock and *ALCAM*$^{-/-}$ cell at an MOI of 0.01 and 0.1 are 1e-5 and 5e-5 respectively. The significant difference is analyzed by two-tailed unpaired Student's *t* test. Source data are provided as a Source Data file.

shaft-HA, knob-HA, shaft-tail-HA and shaft-knob-HA (Fig. 4e). Co-IP analysis showed that full-length fiber, knob domain and shaft-knob domain could interact with ALCAM (Fig. 4e and Supplementary Fig. 10d), suggesting a possibly central role of the knob domain for interaction with ALCAM. Next we sought to determine which domain of ALCAM interacted with fiber and thus constructed ALCAM-C domain-myc and ALCAM-V domain-myc overexpression plasmids. Co-IP analysis showed that ALCAM-C domain could interact with full-length fiber, shaft, knob and shaft-knob while ALCAM-V domain could interact with full-length fiber, knob and shaft-knob (Fig. 4f and Supplementary Fig. 10e). Although ALCAM-C domain seemed to interact with the shaft domain of fiber, no interaction was observed between ALCAM-C domain and tail-shaft construct (Fig. 4f). This suggested that the observed interaction between ALCAM-C and shaft might be experimental artifacts, likely due to the excessive exposure of shaft domain in the non-native shaft-HA overexpression construct. Collectively, these results indicated that the knob domain of fiber could interact with both the C and V domains of ALCAM.

HAdV-B7 internalization is dependent on the DSG-2-ALCAM-EndoA3 axis

Next we explored the in-depth mechanism of ALCAM-mediated HAdV-B7 internalization. We first set experiments to exclude the possibility that ALCAM mediated HAdV-B internalization by regulating the expression of DSG-2[12]. It was found that *ALCAM* knockout did not affect DSG-2 mRNA expression, nor did *DSG-2* knockout affect ALCAM mRNA

https://doi.org/10.1038/s41467-024-55261-3

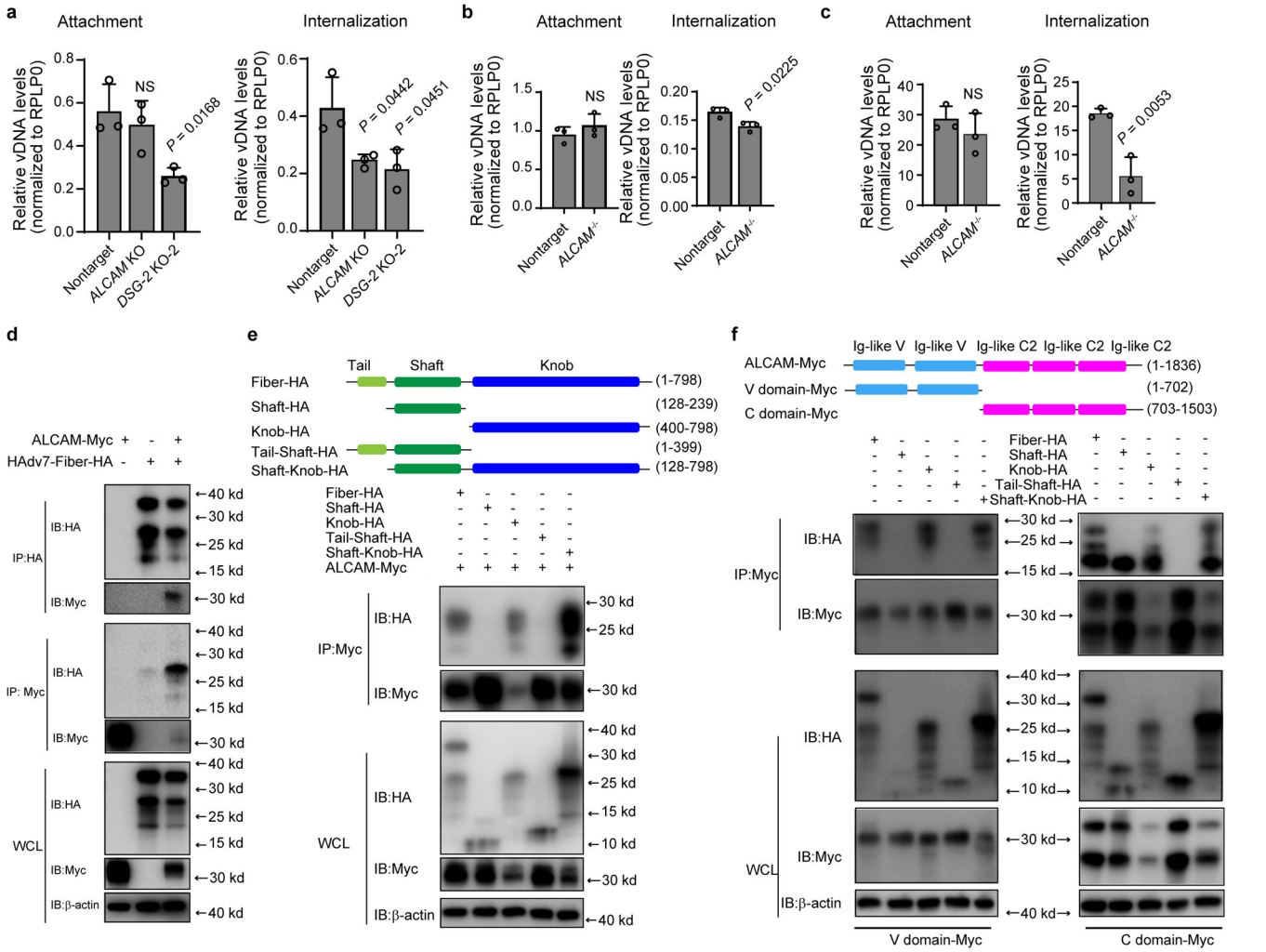

Fig. 4 | Investigation of the function of ALCAM as a functional receptor for HAdV-B7. a Evaluation of the effects of ALCAM and DSG-2 knockout (mixed knockout population) on HAdV-C5/B7-GFP attachment and internalization. HAdV-C5/B7-GFP at an MOI of 20 is incubated with cells on ice for 1 h in the absence (attachment assay) or presence (internalization assay) of a follow-up incubation at 37 °C for 45 min. L3 genomic DNA of attached or internalized viruses is quantified by qPCR. Evaluation of the attachment and internalization of HAdV-C5/B7-GFP (**b**) and clinical HAdV-B7 (**c**) in non-targeting sgRNA mock cells and ALCAM$^{-/-}$ cells. **d** Co-IP analysis of cell lysates from HEK-293T cells co-transfected with ALCAM-myc and HAdV7-fiber-HA overexpression plasmids. **e** Co-IP analysis of the interaction between ALCAM-myc and different domains of fiber protein, including the full-length fiber-HA, shaft-HA, knob-HA, tail-shaft-HA, or shaft-knob-HA. **f** Co-IP analysis of the interaction between ALCAM-C-domain-myc or ALCAM-V-domain-myc and HAdV7-fiber-HA, shaft-HA, knob-HA, tail-shaft-HA or shaft-knob-HA. For (**e**–**f**), immunoprecipitation is conducted using anti-myc beads. For (**d**–**f**), WCL, whole cell lysate. The experiment is repeated three times independently and similar results are obtained. For (**a**–**c**), data are presented as mean ± SD ($n = 3$) from three independent biological replicates. The significant difference between non-targeting and knockout groups is analyzed by two-tailed unpaired Student's t test. Source data are provided as a Source Data file.

expression (Supplementary Fig. 11a, b). We also have quantified the cell surface protein expression of DSG-2 and ALCAM on these knockout cells by flow cytometry and found that DSG-2 and ALCAM proteins expression was mutually independent (Supplementary Fig. 11c, d).

Importantly, the endocytosis of ALCAM has been reported to be dependent on endophilin-A3 (EndoA3)[37]. Thus we sought to investigate the effects of ALCAM-EndoA3 axis on HAdV-B internalization. We conducted *EndoA3* knockout on wild-type (*ALCAM*$^{+/+}$) and *ALCAM*$^{-/-}$ HEK-293A cells respectively (Supplementary Fig. 11e). It was found that *EndoA3* knockout or *ALCAM* knockout alone could reduce HAdV-B7 infection, and dual knockout of *EndoA3* and *ALCAM* did not confer cells additional resistance to HAdV-B7 infection as compared to single knockout alone (Fig. 5a). These results suggested that HAdV-B7 internalization was dependent on the ALCAM-EndoA3 axis.

In order to dissect the functional relation between DSG-2 and ALCAM, we conducted *ALCAM* knockdown (Supplementary Fig. 11f) in wide-type and *DSG-2* knockout HEK-293A cells and challenged these cells with clinical HAdV-B7 infection. The results showed that *ALCAM* knockdown did not have additive effects in *DSG-2* knockout cells for HAdV-B7 infection (Fig. 5b). Overall, these results suggested that DSG-2 and ALCAM could act in the same pathway during HAdV-B7 infection and that ALCAM functioned as an internalization co-factor in the DSG-2-ALCAM-EndoA3 axis for virus attachment and internalization.

Characterization of the binding between ALCAM and knob domain of HAdV-B7 fiber

Since Co-IP experiments revealed interactions between ALCAM and knob domain, we next aimed to characterize the direct binding between ALCAM and knob domain using surface plasmon resonance (SPR). We expressed and purified his-tagged knob domain protein from insect cells (Supplementary Fig. 12a), and then confirmed the identity of the target protein band by mass spectrometry (Supplementary Fig. 12b). HAdV-B7 knob domain was titrated (analyte) on to a

https://doi.org/10.1038/s41467-024-55261-3

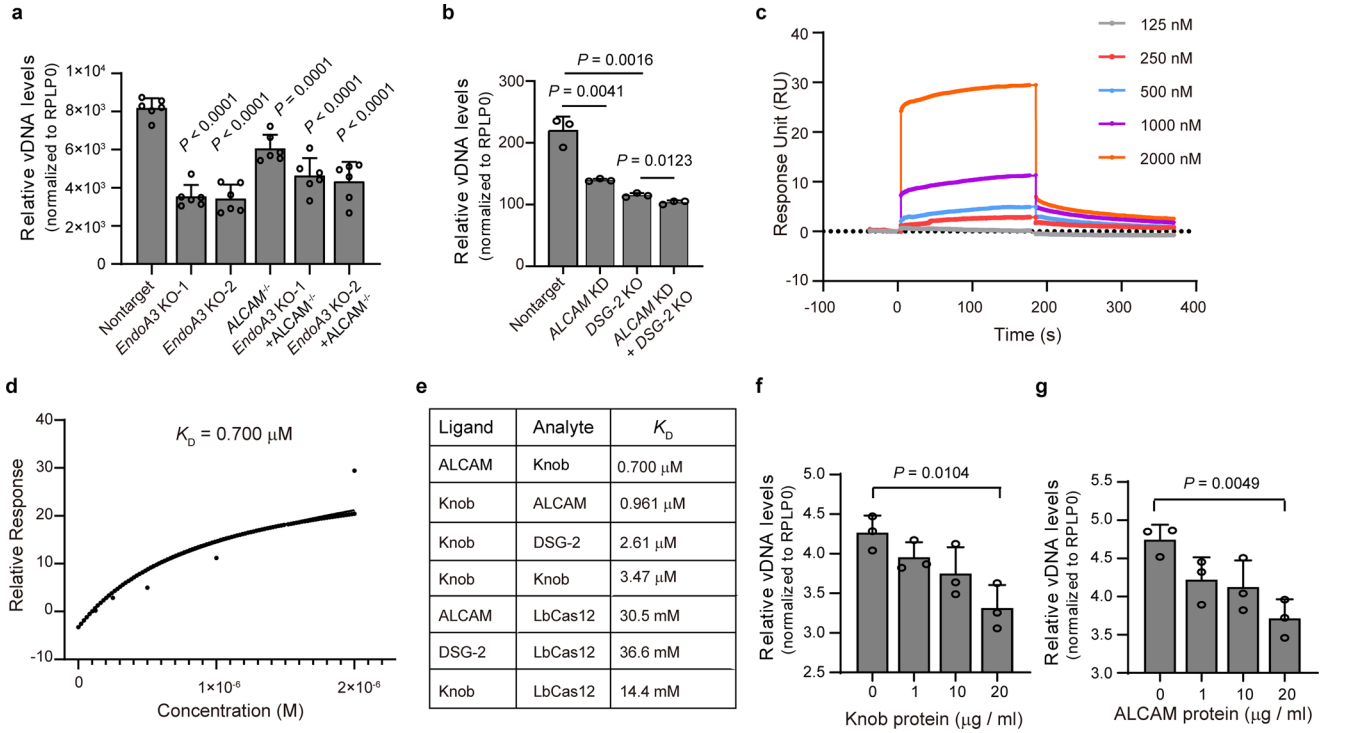

Ligand	Analyte	K_D
ALCAM	Knob	0.700 μM
Knob	ALCAM	0.961 μM
Knob	DSG-2	2.61 μM
Knob	Knob	3.47 μM
ALCAM	LbCas12	30.5 mM
DSG-2	LbCas12	36.6 mM
Knob	LbCas12	14.4 mM

Fig. 5 | Dissection of the mechanism of action of ALCAM-mediated HAdV-B7 internalization. a Analysis of the role of ALCAM-EndoA3 axis in HAdV-B7 (clinical isolate) internalization. HAdV-B7 L3 DNA is quantified in non-targeting, EndoA3 knockout-1, EndoA3 knockout-2, ALCAM-/-, Endo A3/ALCAM dual knockout-1 and Endo A3/ALCAM dual knockout-2 cells at 48 h post infection. **b** Analysis of the individual and combinatorial effects of DSG-2 and ALCAM depletion on clinical HAdV-B7 infection. HAdV-B7 L3 DNA is quantified in non-targeting, *ALCAM* knockdown, *DSG-2* knockout-2, *DSG-2* knockout/*ALCAM* knockdown cells at 48 h post infection of HAdV-B7 infection. **c**, **d** Analysis of the interaction between ALCAM (ligand) and HAdV-B7 knob domain (analyte) using SPR with Biacore 8 K. **c** Association and dissociation curves. **d** Curve-fitting using a steady-state affinity method with constant Rmax analysis. **e** Summary of the determined K_D values for different partner proteins. Evaluation of the effects of fiber knob (**f**) and ALCAM (**g**) proteins on blocking HAdV-B7 infection in wide-type HEK-293A cells. **f** HEK-293A cells are pre-treated with fiber knob protein for 30 min and then incubated with HAdV-B7. **g** HAdV-B7 is pre-treated with ALCAM protein and then supplemented into HEK-293A cells. For (**f**, **g**), HAdV-B7 fiber DNA is quantified by qPCR at 45 min after incubation. For (**a**, **b** and **f**, **g**), data are presented as mean ± SD ($n \geq 3$) from independent biological replicates. The significant difference is analyzed by two-tailed unpaired Student's *t* test. For (**a**), the *p* values between on-targeting, EndoA3 knockout-1, EndoA3 knockout-2, Endo A3/ALCAM dual knockout-1 and Endo A3/ALCAM dual knockout-2 cells cell are 5e-8, 1e-7, 8e-6, and 8e-6 respectively. Source data are provided as a Source Data file.

commercially available ALCAM protein that was immobilized on a CM5 chip (ligand). The knob showed concentration-dependent binding to ALCAM (Fig.5c). The dissociation constant between ALCAM and HAdV-B7 knob domain (K_D) was determined to be in the sub-micromolar range (0.7 μM) (Fig. 5c, d). A biological replicate (Supplementary Fig. 12c) gave a similar K_D value of 0.849 μM. Switching the ligand to knob and analyte to ALCAM also resulted in a similar K_D value of 0.961 μM (Fig. 5e and Supplementary Fig. 12d). SPR experiments with knob (ligand) against DSG-2 (analyte) resulted in a K_D values of 2.61 μM (Fig. 5e and Supplementary Fig. 12e), several fold greater than the value between knob and ALCAM. Knob (ligand) against knob (analyte) resulted in a K_D value of 3.47 μM (Supplementary Fig. 12f), which reflected the interactions between oligomerized knob proteins[38]. In addition, we used an irrelevant *Lachnospiraceae bacterium ND2006*-derived nuclease protein LbCas12a as a negative control, and found that LbCas12 exhibited little binding with ALCAM, DSG-2 or knob (Supplementary Fig. 12g–i).

Next, we investigated whether HAdV-B7 internalization could be blocked by HAdV-B7 fiber knob or ALCAM protein. It was found that pre-incubation of HEK-293A cells with 0.8 μM HAdV-B7 fiber knob protein significantly inhibited HAdV-B7 infection, similar to previous studies with HAdV-B3 and B35 infection[12,15] (Fig. 5f). More importantly, 0.4 μM ALCAM protein could neutralize HAdV-B7 and prevented its infection in HEK-293A cells (Fig. 5g). These results suggested that blocking the interactions between ALCAM and HAdV-B7 fiber knob could restrict viral infection.

Discussion

In this study, we focused on the investigation of SCAP-associated species B HAdV infection. We aimed to understand the connection between the presence of HAdV-B in SCAP patients and the receptor expression profile in patients. In consistency with the inability of DSG-2 deletion to abolish HAdV-B infection in vitro[12], DSG-2 expression in the blood samples did not differ between SCAP patients with and without HAdV-B infection (Fig. 1b). The missing link between DSG-2 expression and HAdV-B infection prompted the investigation of other possible HAdV-B host factors in the present study. Using SfCRISPR-v1 and SfCRISPR-v2 libraries, we consistently identified ALCAM as the top hit. Most importantly, SCAP patients with HAdV-B infection exhibited significantly higher ALCAM expression than those without HAdV-B.

ALCAM functions as a type I transmembrane protein with a large extracellular domain[39]. ALCAM can mediate homophilic adhesion through its V and C domains[40] and influence tumor cell migration via N-glycosylation[41–43]. ALCAM also plays a role in non-clathrin-mediated endocytosis[37] and can promote inflammation and stress in lung injury models[44]. Interestingly, experiments with chimeric and live HAdVs showed that ALCAM functioned as a widely used host factor for both B1 and B2 clusters of HAdV-B. Moreover, ALCAM appeared to promote the infection of HAdV-B viruses that were reported to use either CD46 (B11 and B50) or DSG-2 (B3, B7, B11, and B14) as the primary receptor (Fig. 3a). Along with the attachment and internalization experiments and SPR analyses, these results established ALCAM as a widely used internalization factor across HAdV-B viruses. It would be interesting to

explore in future studies how ALCAM exerts its function together with DSG-2 or other receptors to facilitate the infection of each HAdV-B virus. Interestingly, in contrast to other examined species B viruses, chimeric and clinical HAdV-B35 virus did not have reduced infection on *ALCAM* knockout cells (Fig. 3a and e). It was noted that *ALCAM* knockout slightly decreased cell proliferation (Supplementary Fig. 7d) and slightly increased HAdV-C5 infection. These data suggested that some indirect effects of *ALCAM* knockout on cell proliferation, rather than on virus infection itself, might interfere with the phenotypical analyses of HAdV-B35 infection.

One technical challenge to investigate the function of ALCAM in HAdV-B infection was that *ALCAM* knockout appeared to have some impact on cell growth and proliferation. We thus used competition experiments to alleviate the interference of the effects of ALCAM deletion on cell proliferation (Fig. 2). Related with this, we had difficulties to construct mouse model of constitutive *ALCAM* knockout. In future studies, mice with conditional *ALCAM* knockout can be helpful to uncover the function of ALCAM during in vivo HAdV-B infection.

Another important discovery in our study was that HAdV-B7 knob appeared to interact with both the V- and C-domains of ALCAM (Fig. 4f). This observation raised an interesting question on the pattern of interactions between ALCAM and HAdV-B7 knob. For CAR and CD46 receptors, they both interact with HAdV knob protein in a 3-to-3 mode, where three molecules of receptors interact with knob trimer[45–47]. For DSG-2, however, a single receptor molecule interacts with knob trimer[48–52]. Comparing the K_D of ALCAM and HAdV-B7 knob binding (0.7 μM) with the K_D of DSG-2 and HAdV-B7 knob binding (Fig. 5), it appeared that ALCAM has higher affinity with knob. It was noted that a previous study reported a K_D value of 67 μM for DSG-2 and HAdV-B3 knob[52]. This discrepancy could be explained by the difference between B7 knob and B3 knob or the difference between experimental conditions across different studies. Further investigation including structural analyses should be carried out to explore the unique pattern of interactions between ALCAM for HAdV-B knob.

Moreover, although our data suggested the existence of DSG-2-ALCAM-EndoA3 axis for HAdV-B infection (Fig. 5a, b), it was noted that dual depletion of DSG-2 and ALCAM did not abolish virus infection. These data suggested that HAdV-B might have sophisticated receptor usage profile and that other pathways or proteins might exist for virus attachment or internalization. In line with these results, although gain-of-function and loss-of-function studies confirmed the dependency of HAdV-B infection on ALCAM expression (Fig. 3 and Supplementary Fig. 9), ALCAM expression may not be the only determinant for HAdV-B infection. For example, A549 had similar ALCAM expression as compared to other examined cell types but exhibited much higher susceptibility to HAdV-B infection (Supplementary Fig. 9a, b).

It has been reported that the interaction between HAdV-B3 fiber knob protein and DSG-2 triggers the opening of epithelial junctions in the airway epithelium, which can facilitate the spread of viruses[53,54]. ALCAM is a cell adhesion molecule, bearing a similar function with DSG-2 in cell aggregation. It has been found that ALCAM can mediate cell-to-cell viral transmission during HIV infection[55]. Although we did not observe ALCAM-mediated cell aggregation or cell fusion during HAdV infection in the present study, it would be interesting to explore the functions of ALCAM other than receptor in HAdV-B infection in future studies.

Methods

Clinical study and ethics

The multi-center SCAP study was approved by the Ruijin Hospital Ethics Committee under permit number 2017-186, with informed consent obtained from all patients, who agreed to participate without receiving compensation. All adult patients included in this study were derived from our previously conducted cohort[8,26]. A total of 298 adult patients from 17 hospitals met the enrollment criteria. Of these, 275 (92.3%) were included in the final analysis, with 199 (72.4%) being male, and a median age of 61 years. All experiments were performed and information released according to the instructions of this permit.

Cell culture

HEK-293A cells were purchased from Procell (Cat. No. CL-0003) and HEK-293T (Cat. No. SCSP-502) and CHO-K1 cells (Cat. No. MD12) were obtained from the Cell Bank of Shanghai Institutes for Biological Science (SIBS). HeLa (CRL-1958), A549 (HTB-14) and U-87MG (CCL-185) cells were obtained from the American Type Culture Collection (ATCC). HEK-293A, A549, HEK-293T, HeLa and U-87MG cells were grown in Dulbecco's modified Eagle's medium (DMEM, Thermo) supplemented with 10% fetal bovine serum (FBS, Thermo) and 1% penicillin-streptomycin (Thermo). CHO-K1 cells were grown in F-12K medium (Thermo) supplemented with 10% fetal bovine serum (FBS, Thermo) and 1% penicillin-streptomycin (Thermo). All cells were maintained at 37 °C in a fully humidified incubator containing 5% CO_2. All cells were confirmed by PCR to be free of mycoplasma contamination.

Lentivirus packaging and transduction

For lentivirus (LVs) packaging, HEK-293T cells at a coverage of 70%–90% were transfected with LV envelope plasmid pMD2.G, packaging plasmid psPAX and transfer plasmid pLentiCRISPR-v2 that carried a single sgRNA or pooled sgRNA plasmid library, or transfer plasmid that carried overexpression genes (pLenti-EF1α-IRES-ALCAM-scarlet) (m/m/m, 1.5:1:2) using Lipofectamine 3000 (Thermo, Massachusetts, USA). At 5 to 6 h after transfection, the medium was replaced with fresh medium. The medium supernatant containing LVs was harvested at 48 h to 60 h post transfection by centrifugation at 2000 rpm (500 × *g*)) for 10 min, filtrated through a 0.45-μm filter (Merck, Darmstadt, Germany) and stored at −80 °C.

HEK-293A cells at a coverage of 80%–90% were transduced with LVs in the presence of polybrene (10 μg/ml, Merck) using spinfection through centrifugation at 2000 rpm (500 × *g*) for 2 h. At 12 to 24 h post infection, LV-containing medium was removed and cells were passaged at a ratio of 1:3 to 1:5 and cultured in fresh medium in the presence of 1–2 μg/mL puromycin (Thermo) for 3 to 5 days to remove empty cells containing no LVs or for further fluorescence-positive cell sorting using flow cytometry. Finally, survived cells or sorted cells were collected, aliquoted and stored in liquid nitrogen.

Design and construction of SfCRISPR library

Similar to the design of SfCRISPR-v1 library in our previous work[23], sgRNAs in SfCRISPR-v2 library were designed to target to protein coding regions (NCBI CCDS data, released on 8-Sep-2016)[29] and optimized by two steps. Off-target scores were calculated according on an established algorithm[31], and on-target scores were calculated by Rule Set 2[30]. SgRNA were ranked by on-target scores, and the top 4 sgRNAs with off-target scores of less than 20 were obtained for each gene. The final SfCRISPR-v2 library contained 22,300 sgRNAs targeting to 5622 genes, in comparison to SfCRISPR-v1 library[23] that contained 16,975 sgRNAs targeting to 1314 surface protein genes.

To construct SfCRISPR-v1 and -v2 libraries in HEK-293T, the cells were transduced with LV libraries at an MOI of 0.3 using spinfection as described above. Cells of more than 500-fold coverage of the library size (number of sgRNAs) were collected, aliquoted and stored in liquid nitrogen.

CRISPR screening for HAdV-C5/B7 host factors and next-generation sequencing (NGS) analyses of sgRNA enrichment

HEK-293T cell library was infected with HAdV-C5/B7 carrying an EGFP transgene (HAdV-C5/B7-EGFP) at an MOI of 0.0001 for 48 h. Then the cells were harvested and EGFP-negative cells were sorted using flow cytometry (Moflo, Beckman Coulter, California, USA). Genomic DNA of

the sorted EGFP-negative cells was extracted using phenol: chloroform: isoamyl alcohol (v/v/v, 25:24:1), and then DNA was purified using ethanol precipitation. Genome-integrated sgRNAs were amplified from the collected genomic DNA by PCR using primers containing Illumina adaptors (Supplementary Table 1). The sequences of PCR products were analyzed using NGS on Illumina HiSeq 3000 platform by Genewiz (Suzhou, Jiangsu, China). The raw read counts of NGS were subjected to MAGeCK analyses to determine the enriched sgRNA and gene knockouts. A false discovery rate (FDR) of less than 0.05 was used as cut-off to determine significantly enriched sgRNAs and candidate genes.

HAdV-C5 and HAdV-C5/B7 production and infection

HAdV-C5 was generated using AdMax recombinant system (MicroBix Biosystems) with the helper plasmid pBHG-cre-ΔE1Δ3-loxp and transgene plasmid pHBAd-GFP. For HAdV-C5/B7 production, the shaft and knob domains of fiber of HAdV-C5 in helper plasmid pBHGloxΔE1-3-CRE were replaced with those of C5-based chimeric HAdV-B7, -B3, -B35, -B11, -B14 and -B50 to obtain pBHGloxΔE1-3-CRE-B7 fiber, -B3 fiber, -B35 fiber, - B11 fiber, -B14 fiber and -B50 fiber (Supplementary Table 2). For HAdV packaging, HEK-293A cells at a confluent of 70–90% were transfected with pHBAd-GFP and pBHGloxΔE1-3-CRE, pBHGloxΔE1-3-CRE-B7 fiber, -B3 fiber, -B35 fiber, - B11 fiber, -B14 fiber, or -B50 fiber (m/m, 1:1) using Lipofectamine 3000 (Thermo). At 5 to 6 h post transfection, the medium was replaced with fresh medium. At 48 to 72 h after transfection, the cells were collected and subjected to three rounds of freeze-thaw cycles, and cracked cells were centrifuged at 200 rpm for 5 min in 4 °C. Cell debris was discarded and the supernatants were centrifuged at 3200 rpm (1000 × *g*) for 15 min in 4 °C. The supernatants including HAdVs were collected, aliquoted and stored in −80 °C. Virus titers were determined by the 50% tissue culture infectious dose ($TCID_{50}$) assay.

For HAdV infection, HEK-293A cells were seeded on to 24- and 12-well plates at a density of 1.5×10^5 and 3.0×10^5 cells per well, respectively. Unless noted, at 24 h after seeding, cells were infected with HAdV-C5 or HAdV-C5/B7 at an MOI of 0.002 for 2 h, washed with PBS for three times and then cultured in fresh medium for 48 h.

Generation of CRISPR-Cas9 knockout cells

The lentiviral transfer plasmids pLentiCRISPR-v2-sgRNA carrying single sgRNA were generated as previously described[28] Briefly, plentiCRISPR-v2 vector was digested with Esp3I (Thermo), and then annealed forward and reverse oligonucleotides encoding 20 bp sgRNA target sequence (Supplementary Table 3) were ligated into digested vector and chemically transformed into DH5α *E. coli* (Tsingke, Beijing, China).

The LVs were packaged and transduced into cells as described above. To evaluate the knockout efficiency, the genomic DNA of knockout cells were extracted using Quick Extraction kit (Lucigen) and the genomic sites of targeted genes were PCR amplified using corresponding primers (Supplementary Table 4). The PCR products were sequenced by Sanger sequencing (Genewiz) and gene knockout efficiency was analyzed by TIDE website (https://tide.nki.nl/)[56]. Single clones were obtained by single cell sorting using flow cytometry (Moflo, Beckman) and genotyped by Sanger sequencing to determine the mutations at each allele. Only clones with both alleles containing out-of-frame indels were selected. WB and flow cytometry analysis were used to characterize the protein expression in the selected clones.

RT-qPCR

Total RNA from cultured cells or infected cells was extracted using TRIzol (Thermo), chloroform (Titan) and purified using isopropanol precipitation. RNA was then reverse transcribed into cDNA by PrimeScript RT reagent Kit with gDNA Eraser (Takara Bio Inc., Shiga, Japan). The mRNA levels were quantified by reverse transcription quantitative PCR (RT-qPCR) using SYBR green dye and specific primers (Supplementary Table 5) on Applied Biosystems Q6 Real-Time PCR cycler (Thermo). Each group contained three biological replicates and each biological replicate contained two technical replicates. The variations between technical replicates were controlled within 2% of Ct (cycles of threshold) value. The mean values of the technical replicates were recorded. For the biological replicates, the day-to-day or person-to-person variations were typically controlled to be below 10% (90–110% of the mean values). All SYBR Green primers were validated with dissociation curves. The expression of genes was normalized to RPLP0 or β-actin.

qPCR quantification of HAdV genome

Genomic DNA of HAdV or HAdV-containing cells was extracted using phenol: chloroform: isoamyl alcohol (v/v/v, 25:24:1) and then purified using ethanol precipitation. Virus DNA level was determined by quantitative PCR (qPCR) using SYBR green dye and specific primers (Supplementary Table 5) on Applied Biosystems Q6 Real-Time PCR cycler (Thermo). All SYBR Green primers were validated with dissociation curves. The genomic DNA level was normalized to β-actin.

siRNA knockdown experiments

Cultured HEK293-A cells of 5×10^5 were seeded on to 6-well plates. At 24 h after seeding, 100 pmol siRNA (Genepharma, Shanghai, China) (Supplementary Table 6) was transfected using 7.5 μL Lipofectamine 2000 (Thermo) for 6 h, then washed with PBS and cultured in fresh DMEM (Thermo) supplemented with 10% fetal bovine serum (FBS, Thermo). At 48 h post transfection, cells were infected with HAdV at an MOI of 0.001 for 24 h. The cell samples were harvested and lysed for virus DNA extraction as described above.

Virus attachment and internalization assays

HEK-293A cells were seeded on to 12-well plates pre-treated with 0.1 mg/ml poly-D-lysine (Meilunbio, China) at a density of 200,000 cells per well and incubated overnight. For virus attachment assay, cells were incubated with HAdV at an MOI of 20 in cold medium without FBS on ice for 60 min, then washed with cold Dulbecco's phosphate-buffered saline (DPBS) for three times without protease treatment and harvested. Virus DNA was extracted from the cells containing attached virus and quantified by qPCR as described above.

For virus internalization assay, cells were incubated with HAdV at an MOI of 20 in cold medium on ice for 60 min, washed with cold DPBS for three times, treated with pre-warmed medium containing FBS and then incubated at 37 °C for 45 min. The treated cells were washed with PBS for three times and then treated with 0.25% trypsin (Thermo, Cat. No. 25200072) for 30 s to remove surface-bound virus particles. Internalized viruses, including both endosomal and cytoplasmic portions, were quantified by qPCR as described above.

Competitive infection assays

HEK293-A knockout cell lines and HEK293-A WT cells expressing red fluorescence protein were pre-mixed (1:1) and seeded on to 12-well plates. A 24 h after seeding, the cells were incubated with recombinant HAdV-GFP at an MOI of 0.001 for 2 h, washed with PBS for 3 times and incubated in fresh DMEM (Thermo) supplemented with 10% fetal bovine serum (FBS, Thermo). At 24, 48, and 72 h post infection, cells were harvested and resuspended in PBS. Flow cytometry (CytoFLEX S, Beckman) was used for quantification of infected cells using green fluorescence and the collected data were analyzed by Flowjo (Version 10.4). For test groups (*ALCAM* knockout), GFP positive rate was calculated based on the RFP-negative population. For the control groups (wild type), GFP positive rate was calculated based on the RFP-positive population.

Construction of stable cell lines harboring overexpressed genes

Human and hamster ALCAM genes were codon-optimized for expression in human cells and synthesized by Genewiz (Supplementary Table 7–8). The 20 bp sgRNA-targeting sites and PAM sequences of Human ALCAM gene were mutated with silent mutations. Myc and FLAG tags were added to the C-terminus of these genes for WB detection. These genes were cloned into the XbaI and BamH1 sites of pLV-EF1α-IRES-zsgreen plasmid. The transgene-containing LVs was packaged as described above and then transduced into ALCAM$^{-/-}$ cells. The transduced cells were sorted using flow cytometry (Moflo, Beckman), collected, aliquoted and stored in liquid nitrogen.

WB analysis

For WB analyses, cells were lysed with RIPA buffer (thermo) on ice for 30 min and centrifuged at 12,000 rpm (13,523 × *g*) at 4 °C for 10 min to remove cell debris. The total protein concentration was determined using BCA Protein Assay Kit (Beyotime Biotechnology, Beijing, China). Cell lysate was mixed with SDS-PAGE loading buffer (thermo) containing 200 mM DTT, incubated at 95 °C for 10 min and resolved on 4–12% PAGE gels (GenScript, Nanjing, China). Protein samples were transferred onto polyvinylidene fluoride (PVDF) membranes (Merck) with a pore size of 0.45 μm using a gel transfer system (Bio-rad, California, USA). The following primary and secondary antibodies were used in WB including anti-Myc rabbit antibody (CST, Cat. No. 2272S), anti-HA rabbit antibody (CST, Cat. No. 3724S), anti-ALCAM rabbit antibody (SinoBiological, Cat. No. 80221-RP02), HRP-conjugated anti-mouse IgG (CST, Cat. No. 7076S), HRP-conjugated anti-rabbit IgG (CST, Cat. No. 5127S). Anti-β actin antibody conjugated with HRP (CST, Cat. No. 5125S) was used as an internal control.

Co-Immunoprecipitation (Co-IP)

HEK-293T cells were seeded on to 6-well plates at a density of 1×10^6 cells per well. After the confluency reached 70–80%, plasmid was transfected into cells. Plasmids containing Myc-labeled ALCAM, ALCAM-C domain or ALCAM-V domain (Supplementary Table 7) and plasmids containing HA-labeled fiber proteins or its truncation constructs (Supplementary Table 9) were co-transfected into HEK-293T cells by Lipofectamine 3000 (Thermo). At 24 h after transfection, cells were resuspended with RIPA lysis buffer (Thermo) and NP-40 lysis buffer (Thermo) for WB and immunoprecipitation, respectively. NP-40 lysates were incubated with magnetic beads (Thermo) containing anti-HA or anti-Myc antibody at room temperature for 2 h. Magnetic beads were collected with a magnetic rack (Thermo), then proteins bound to the magnetic beads were eluted by 1×SDS-PAGE loading buffer containing DTT. Finally, total proteins and co-immunoprecipitated proteins were detected by WB as described above.

Flow cytometry analysis

To determine the cell surface expression of ALCAM, CAR and DSG-2, wide-type, ALCAM knockout, CAR knockout and DSG-2 knockout HEK-293A cells were stained with the indicated antibodies. Cells were blocked with 5% BSA for 1 h, incubated with primary antibodies for 1 h and then with secondary antibodies for 1 h. The following primary and secondary antibodies were used including anti-ALCAM rabbit antibody (SinoBiological, Cat. No. 80221-RP02), anti-DSG-2 rabbit antibody (CST, Cat. No. 88970S), anti-CAR rabbit antibody (Abcam, Cat. No. ab272711), anti-rabbit IgG (CST, Cat. No. 5127S), Alexa Fluor 568 conjugated anti-Rabbit IgG (Thermo, Cat. A-10042), Alexa Fluor 647 conjugated anti-Mouse Rabbit IgG (Thermo, Cat. A-31571). All samples were run on CytoFLEX (Beckman) and FlowJo software was used to analyze the data.

Expression and purification of the knob domain of HAdV7

Knob domain was synthesized and cloned into pFastBac vector plasmid (Supplementary Table 10). The recombinant pFastBac1-knob plasmid was transformed into DH10Bac competent cells, and the white single colonies with recombinant bacmid were picked for overnight culturing. Then recombinant bacmids including knob gene were isolated and purified. For recombinant baculovirus packaging, the bacmid of knob was transfected into Hi-5 insect cells, and the medium supernatant was collected at 72 h after transfection. The medium supernatant was centrifuged at 1000 *g* for 10 min at 4 °C to remove cell debris and the supernatant was harvested as initial virus (P1). After two cycles of amplification of P1 virus in Sf-9 cells, P3 virus was obtained. For knob expression, Sf9 cells were infected with P3 virus, and cell pellets were collected at 48 h post infection.

For protein purification, the cell pellets were lysed with homogenizing buffer containing 20 mM Tris, pH 7.5, 500 mM NaCl, 10% glycerol, Triton X-100, protease inhibitor cocktail and nuclease. The cell lysate was centrifuged at 12,000 rpm (13,523 × *g*) for 30 min at 4 °C and the supernatant was isolated. The lysate supernatant was collected and loaded onto Ni column in loading buffer containing 20 mM Tris, pH 7.5, 500 mM NaCl and 50 mM imidazole. Proteins were eluted with elution buffer that was made by supplementing loading buffer with 500 mM imidazole. Eluted protein samples were further purified and buffer-exchanged to storage buffer containing 20 mM Tris, 300 mM NaCl, pH 7.5 and 10% glycerol, aliquoted and stored at −80 °C.

Mass spectrometry validation of purified knob protein

The purified knob protein was validated by Orbitrap Fusion MS (Thermo Fisher, San Jose, CA) using Proteome Discoverer 2.2 and X calibur analysis software at the Analytical Chemistry Platform at SIAIS, ShanghaiTech University.

Surface plasmon resonance (SPR) experiment

To determine the binding affinity of knob with ALCAM (Sino, Cat. No. 10045-H08H-100), DSG-2 (MCE, Cat. No. HY-P77917) or knob, the SPR assay was carried out. We performed SPR experiments with a Biacore 8 K (Cytiva) instrument. All assays were performed with a running buffer containing PBS with 0.05% Tween-20 and 0.1% BSA. ALCAM, DSG-2 and B7 fiber knob were immobilized on the active flow cell 2 (FC2) of 1 of the 8 channels of a Series S Sensor Chip CM5 using standard amine coupling reagents 1-ethyl-3-(3-dimethylaminopropyl) carbodiimide (EDC) and N-hydroxysuccinimide (NHS) (Cytiva, Marlborough, MA, USA), and flow cell 1 (FC1) was used as a reference flow cell. The excess activated carboxyls was blocked using ethanolamine. Three samples and LbCas12a (negative control) containing only running buffer were flowed over both reference flow cell (FC1) and immobilized FC2 followed by 2-fold serial dilutions of analyte (ALCAM, DSG-2 or B7 fiber knob) (30 ml/min, association 180 s, dissociation 180 s). The chip surface was regenerated by the removal of analyte with a regeneration buffer. All the binding data were double referenced by blank cycle and reference flow cell subtraction. Binding curves were displayed, and the dissociation constants (K_D) for the interaction were determined using the steady-state affinity method in the Biacore 8 K Evaluation Software Version 3.0 (Cytiva).

Blocking assays with fiber knob or ALCAM protein

HEK-293A cells were seeded on to 12-well plates pre-treated with 0.1 mg/ml poly-D-lysine (Meilunbio, China) at a density of 200,000 cells per well and incubated overnight. For fiber knob blocking assay, cells were pre-incubated with HAdV-B7 fiber knob protein at concentrations of 0, 1, 10, and 20 μg/ml for 30 min, and then cells were infected by HAdV-B7 at an MOI of 20 and incubated for another 45 min.

For ALCAM blocking assay, HAdV-B7 was pre-incubated with ALCAM protein at concentrations of 0, 1, 10, and 20 μg/ml for 30 min, and then virus-ALCAM mixture were added to cells and incubated for another 45 min. The treated cells were washed with PBS for three times and then treated with 0.25% trypsin (Thermo, Cat. No. 25200072) for 30 s to remove surface-bound virus particles. Cells containing

internalized virus was lysed and virus DNA was extracted for qPCR quantification as described above.

Statistics and reproducibility

All data were the results from at least three biological replicates within one-month time frame and shown as mean ± standard deviation unless noted otherwise. Sample size of biological replicates was selected as at least three to examine experimental variations. No data were excluded for analyses. Statistical analyses and graphing were performed with GraphPad Prism 7.0. The *P* values were determined using two-tailed unpaired Student's t-test or two-way ANOVA with Sidak's multiple comparisons test unless otherwise noted.

Reporting summary

Further information on research design is available in the Nature Portfolio Reporting Summary linked to this article.

Data availability

The authors declare that all data supporting the findings of this study are available in the article, its Supplementary information, its Source Data or from the corresponding authors upon request. Source data are provided with this paper. The NGS data used in this study are available in the SRA database under the accession code PRJNA1164007. The raw sequencing data for human blood transcriptomics can be found in the Genome Sequence Archive (GSA, https://ngdc.cncb.ac.cn/gsa-human) database under the accession code HRA009475. Source data are provided with this paper.

References

1. Greber, U. F. & Flatt, J. W. Adenovirus entry: from infection to immunity. *Annu. Rev. Virol.* **6**, 177 (2019).
2. Lion, T. Adenovirus infections in immunocompetent and immunocompromised patients. *Clin. Microbiol. Rev.* **27**, 441 (2014).
3. Scott, M. K. et al. Human adenovirus associated with severe respiratory infection, Oregon, USA, 2013-2014. *Emerg. Infect. Dis.* **22**, 1044 (2016).
4. Zeng, S. Z. et al. Persistent viral shedding of human adenovirus type 7 in children with severe pneumonia. *J. Med. Virol.* **93**, 4846 (2021).
5. Wei, J. et al. Genome and proteomic analysis of risk factors for fatal outcome in children with severe community-acquired pneumonia caused by human adenovirus 7. *J. Med. Virol.* **95**, e29182 (2023).
6. Kujawski, S. A. et al. Outbreaks of adenovirus-associated respiratory illness on 5 college campuses in the United States, 2018-2019. *Clin. Infect. Dis.* **72**, 1992 (2021).
7. Pollio, A. R. et al. Clustered cases of human adenovirus types 4, 7, and 14 infections in US Department of Defense Beneficiaries during the 2018-2019 season. *J. Med. Virol.* **95**, e28571 (2023).
8. Qu, J. et al. Aetiology of severe community acquired pneumonia in adults identified by combined detection methods: a multi-centre prospective study in China. *Emerg. Microbes Infect.* **11**, 556 (2022).
9. Bergelson, J. M. et al. Isolation of a common receptor for Coxsackie B viruses and adenoviruses 2 and 5. *Science* **275**, 1320 (1997).
10. Roelvink, P. W. et al. The coxsackievirus-adenovirus receptor protein can function as a cellular attachment protein for adenovirus serotypes from subgroups A, C, D, E, and F. *J. Virol.* **72**, 7909 (1998).
11. Gaggar, A., Shayakhmetov, D. M. & Lieber, A. CD46 is a cellular receptor for group B adenoviruses. *Nat. Med.* **9**, 1408 (2003).
12. Wang, H. et al. Desmoglein 2 is a receptor for adenovirus serotypes 3, 7, 11 and 14. *Nat. Med.* **17**, 96 (2011).
13. Tuve, S. et al. A new group B adenovirus receptor is expressed at high levels on human stem and tumor cells. *J. Virol.* **80**, 12109 (2006).
14. Chitaev, N. A. & Troyanovsky, S. M. Direct Ca2+-dependent heterophilic interaction between desmosomal cadherins, desmoglein and desmocollin, contributes to cell-cell adhesion. *J. Cell Biol.* **138**, 193 (1997).
15. Tuve, S. et al. Role of cellular heparan sulfate proteoglycans in infection of human adenovirus serotype 3 and 35. *PLoS Pathog.* **4**, e1000189 (2008).
16. Wickham, T. J., Mathias, P., Cheresh, D. A. & Nemerow, G. R. Integrins alpha v beta 3 and alpha v beta 5 promote adenovirus internalization but not virus attachment. *Cell* **73**, 309 (1993).
17. Short, J. J., Vasu, C., Holterman, M. J., Curiel, D. T. & Pereboev, A. Members of adenovirus species B utilize CD80 and CD86 as cellular attachment receptors. *Virus Res.* **122**, 144 (2006).
18. Wei, J. et al. Genome-wide CRISPR screens reveal host factors critical for SARS-CoV-2 infection. *Cell* **184**, 76 (2021).
19. Daniloski, Z. et al. Identification of required host factors for SARS-CoV-2 infection in human cells. *Cell* **184**, 92 (2021).
20. Ganaie, S. S. et al. Lrp1 is a host entry factor for Rift Valley fever virus. *Cell* **184**, 5163 (2021).
21. Meertens, L. et al. FHL1 is a major host factor for chikungunya virus infection. *Nature* **574**, 259 (2019).
22. Zhao, X. et al. Human neonatal Fc receptor is the cellular uncoating receptor for enterovirus B. *Cell* **177**, 1553 (2019).
23. Mei, H. et al. Surfaceome CRISPR screen identifies OLFML3 as a rhinovirus-inducible IFN antagonist. *Genome Biol.* **22**, 297 (2021).
24. Arai, F., Ohneda, O., Miyamoto, T., Zhang, X. Q. & Suda, T. Mesenchymal stem cells in perichondrium express activated leukocyte cell adhesion molecule and participate in bone marrow formation. *J. Exp. Med.* **195**, 1549 (2002).
25. Tomko, R. P., Xu, R. & Philipson, L. HCAR and MCAR: the human and mouse cellular receptors for subgroup C adenoviruses and group B coxsackieviruses. *Proc. Natl Acad. Sci. USA* **94**, 3352 (1997).
26. Zhao, J. et al. A multicenter prospective study of comprehensive metagenomic and transcriptomic signatures for predicting outcomes of patients with severe community-acquired pneumonia. *EBioMedicine* **96**, 104790 (2023).
27. Gallardo, J., Perez-Illana, M., Martin-Gonzalez, N. & San Martin, C. Adenovirus structure: what is new? *Int. J. Mol. Sci.* **22**, 5240 (2021).
28. Mei, H. et al. CRISPR-surfaceome: an online tool for designing highly efficient sgRNAs targeting cell surface proteins. *Comput. Struct. Biotechnol. J.* **20**, 3833 (2022).
29. Pruitt, K. D. et al. The consensus coding sequence (CCDS) project: Identifying a common protein-coding gene set for the human and mouse genomes. *Genome Res.* **19**, 1316 (2009).
30. Doench, J. G. et al. Optimized sgRNA design to maximize activity and minimize off-target effects of CRISPR-Cas9. *Nat. Biotechnol.* **34**, 184 (2016).
31. Hsu, P. D. et al. DNA targeting specificity of RNA-guided Cas9 nucleases. *Nat. Biotechnol.* **31**, 827 (2013).
32. Hart, T. et al. Evaluation and design of genome-wide CRISPR/SpCas9 knockout screens. *G3* **7**, 2719 (2017).
33. Tan, E., Chin, C. S. H., Lim, Z. F. S. & Ng, S. K. HEK293 cell line as a platform to produce recombinant proteins and viral vectors. *Front. Bioeng. Biotechnol.* **9**, 796991 (2021).
34. Tian, X. et al. Broadly neutralizing monoclonal antibodies against human adenovirus types 55, 14p, 7, and 11 generated with recombinant type 11 fiber knob. *Emerg. Microbes Infect.* **7**, 206 (2018).
35. Kumar, S., Stecher, G., Li, M., Knyaz, C. & Tamura, K. MEGA X: molecular evolutionary genetics analysis across computing platforms. *Mol. Biol. Evol.* **35**, 1547 (2018).
36. Tamura, K., Stecher, G. & Kumar, S. MEGA11: molecular evolutionary genetics analysis version 11. *Mol. Biol. Evol.* **38**, 3022 (2021).
37. Renard, H. F. et al. Endophilin-A3 and Galectin-8 control the clathrin-independent endocytosis of CD166. *Nat. Commun.* **11**, 1457 (2020).
38. van Raaij, M. J., Mitraki, A., Lavigne, G. & Cusack, S. A triple beta-spiral in the adenovirus fibre shaft reveals a new structural motif for a fibrous protein. *Nature* **401**, 935 (1999).

39. Ferragut, F., Vachetta, V. S., Troncoso, M. F., Rabinovich, G. A. & Elola, M. T. ALCAM/CD166: a pleiotropic mediator of cell adhesion, stemness and cancer progression. *Cytokine Growth Factor Rev.* **61**, 27 (2021).
40. van Kempen, L. C. et al. Molecular basis for the homophilic activated leukocyte cell adhesion molecule (ALCAM)-ALCAM interaction. *J. Biol. Chem.* **276**, 25783 (2001).
41. Ferragut, F. et al. Dual knockdown of Galectin-8 and its glycosylated ligand, the activated leukocyte cell adhesion molecule (ALCAM/CD166), synergistically delays in vivo breast cancer growth. *Biochim. Biophys. Acta Mol. Cell Res.* **1866**, 1338 (2019).
42. Fernández, M. M. et al. Glycosylation-dependent binding of galectin-8 to activated leukocyte cell adhesion molecule (ALCAM/CD166) promotes its surface segregation on breast cancer cells. *Biochim. Biophys. Acta* **1860**, 2255 (2016).
43. Delgado, V. M. et al. Modulation of endothelial cell migration and angiogenesis: a novel function for the "tandem-repeat" lectin galectin-8. *Faseb J.* **25**, 242 (2011).
44. Kim, M. N. et al. A novel regulatory role of activated leukocyte cell-adhesion molecule in the pathogenesis of pulmonary fibrosis. *Am. J. Respir. Cell Mol. Biol.* **66**, 415 (2022).
45. Bewley, M. C., Springer, K., Zhang, Y. B., Freimuth, P. & Flanagan, J. M. Structural analysis of the mechanism of adenovirus binding to its human cellular receptor. *Car. Sci.* **286**, 1579 (1999).
46. Kirby, I. et al. Identification of contact residues and definition of the CAR-binding site of adenovirus type 5 fiber protein. *J. Virol.* **74**, 2804 (2000).
47. Persson, B. D. et al. Adenovirus type 11 binding alters the conformation of its receptor CD46. *Nat. Struct. Mol. Biol.* **14**, 164 (2007).
48. Vassal-Stermann, E. et al. CryoEM structure of adenovirus type 3 fibre with desmoglein 2 shows an unusual mode of receptor engagement. *Nat. Commun.* **10**, 1181 (2019).
49. Hograindleur, M. A. et al. Binding mechanism elucidation of the acute respiratory disease causing agent adenovirus of serotype 7 to desmoglein-2. *Viruses* **12**, 1075 (2020).
50. Wang, H. et al. Structural and functional studies on the interaction of adenovirus fiber knobs and desmoglein 2. *J. Virol.* **87**, 11346 (2013).
51. Vassal-Stermann, E. et al. Mapping of Adenovirus of serotype 3 fibre interaction to desmoglein 2 revealed a novel 'non-classical' mechanism of viral receptor engagement. *Sci. Rep.* **8**, 8381 (2018).
52. Baker, A. T. et al. Diversity within the adenovirus fiber knob hypervariable loops influences primary receptor interactions. *Nat. Commun.* **10**, 741 (2019).
53. Wang, H. et al. Multimerization of adenovirus serotype 3 fiber knob domains is required for efficient binding of virus to desmoglein 2 and subsequent opening of epithelial junctions. *J. Virol.* **85**, 6390 (2011).
54. Beyer, I., van Rensburg, R. & Lieber, A. Overcoming physical barriers in cancer therapy. *Tissue Barriers* **1**, e23647 (2013).
55. Park, R. J. et al. A genome-wide CRISPR screen identifies a restricted set of HIV host dependency factors. *Nat. Genet.* **49**, 193 (2017).
56. Brinkman, E. K. et al. Easy quantification of template-directed CRISPR/Cas9 editing. *Nucleic Acids Res.* **46**, e58 (2018).

Acknowledgements

We thank Y. Zhang from the Discovery Technology Platform at the Shanghai Institute for Advanced Immunochemical Studies (SIAIS), ShanghaiTech University for providing technical support of Biacore8K, thank L.S Zhang and P.W. Zhang from Discovery Technology Platform for the support of flow cytometry experiments, thank W. Zhu from Analytical Chemistry Platform for assistance with mass spectrometry analysis and thank Biomedical Big Data Platform for the design of sgRNA libraries and MAGeCK analyses. This research was supported by National Key Research and Development Program of China (2023ZD0506200 to J.Q.), Major Project of Guangzhou National Laboratory (Grant No. GZNL2024A01014 to J.L.), Shanghai Municipal Key Clinical Specialty (shslczdzk0220 to J.Q.), the Shanghai Top-Priority Clinical Key Disciplines Construction Project (2017ZZ02014 to J.Q.), the Shanghai Key Laboratory of Emergency Prevention, Diagnosis and Treatment of Respiratory Infectious Diseases (20dz2261100 to J.Q.), the Cultivation Project of Shanghai Major Infectious Disease Research Base (20dz2210500 to J.Q.), the Innovative Research Team of High-level Local Universities in Shanghai (to J.Q.), the Science and Technology Commission of Shanghai Municipality (23ZR1442100 to J.L.), and the Shanghai Frontiers Science Center for Biomacromolecules and Precision Medicine at ShanghaiTech University (2022A0301-417-01 to J.L.).

Author contributions

J.Q. and J.L. conceived this study, J.Q., J.L., H.M., and Y.X. designed the experiments, Y.X., H.M., and P.H. carried out the experiments and analyzed the data. W.W., H.M., and J.L. designed the sgRNA libraries, X.T., R.Z., and X.L isolated the clinical HAdV-B7, -B3, -B14 and -B35, Y.X., H.M., J.L and J.Q. wrote the manuscript. All authors contributed to the article and approved the submitted version.

Competing interests

The authors declare no competing interests.

Additional information

Supplementary information The online version contains supplementary material available at https://doi.org/10.1038/s41467-024-55261-3.

Correspondence and requests for materials should be addressed to Jia Liu or Jieming Qu.

Peer review information *Nature Communications* thanks the anonymous reviewers for their contribution to the peer review of this work. A peer review file is available.